JEREMY.SEPINSKY@SCRANTON.EDU, B-WILLEMS, VICKY, AND RASIO@NORTHWESTERN.EDU
Preprint typeset using LaTeX style emulateapj v. 11/10/09

INTERACTING BINARIES WITH ECCENTRIC ORBITS. III. ORBITAL EVOLUTION DUE TO DIRECT IMPACT AND SELF-ACCRETION

J. F. Sepinsky[1,2], B. Willems [2], V. Kalogera[2], F. A. Rasio[2]
[1] The University of Scranton, Department of Physics and Electrical Engineerings, Scranton, PA 18510 and
[2] Department of Physics and Astronomy, Northwestern University, 2145 Sheridan Road, Evanston, IL 60208
jeremy.sepinsky@scranton.edu, b-willems, vicky, and rasio@northwestern.edu

ABSTRACT

The rapid circularization and synchronization of the stellar components in an eccentric binary system at the onset of Roche lobe overflow is a fundamental assumption common to all binary stellar evolution and population synthesis codes, even though the validity of this assumption is questionable both theoretically and observationally. Here we calculate the evolution of the orbital elements of an eccentric binary through the direct three-body integration of a massive particle ejected through the inner Lagrangian point of the donor star at periastron. The trajectory of this particle leads to three possible outcomes: direct accretion onto the companion star within a single orbit, self-accretion back onto the donor star within a single orbit, or a quasi-periodic orbit around the companion star, possibly leading to the formation of a disk. We calculate the secular evolution of the binary orbit in the first two cases and conclude that direct impact accretion can increase as well as decrease the orbital semi-major axis and eccentricity, while self-accretion always decreases the orbital semi-major axis and eccentricity. In cases where mass overflow contributes to circularizing the orbit, circularization can set in on timescales as short as a few per cent of the mass transfer timescale. In cases where mass overflow increases the eccentricity, the orbital evolution is governed by competition between mass overflow and tidal torques. In the absence of tidal torques, mass overflow results in direct impact can lead to substantially subsynchronously rotating donor stars. Contrary to assumptions common in the literature, direct impact accretion furthermore does not always provide a strong sink of orbital angular momentum in close mass-transferring binaries; in fact we instead find that a significant part can be returned to the orbit during the particle orbit. The formulation presented in this paper together with our previous work can be combined with stellar and binary evolution codes to generate a better picture of the evolution of eccentric, Roche lobe overflowing binary star systems.

Subject headings: Celestial mechanics, Stars: Binaries: Close, Stars: Mass Loss, Accretion, Methods: Numerical

1. INTRODUCTION

In close binaries, the combined effects of stellar and orbital evolution can cause a star to fill its Roche lobe and transfer mass to its companion. If the orbit is eccentric this mass transfer is expected to commence at or near the periastron of the binary orbit where the effective Roche lobes of the component stars are smallest (Layton et al. 1998; Sepinsky et al. 2007a; Church et al. 2009; Regös et al. 2005). Until recently, studies of mass transfer in eccentric binaries mainly focused on smoothed particle hydrodynamics calculations of the mass transfer stream and much less on the effects of the mass transfer on secular binary evolution.

To the best of our knowledge, Sepinsky et al. (2007b, 2009) were the first to study in detail the secular evolution of the orbital semi-major axis and eccentricity of eccentric mass-transferring binaries. The authors adopted a perturbation method initially outlined by Hadjidemetriou (1969) and found that, depending on the binary properties at the onset of mass transfer, the orbital semi-major axis and eccentricity can either increase or decrease at a rate linearly proportional the mass transfer rate at periastron. Contrary to common assumptions, tides therefore do not always rapidly circularize binary orbits as a star evolves towards filling its Roche lobe.

Sepinsky et al. (2007b, 2009) calculated the orbital evolution due to mass transfer in eccentric binaries assuming mass transfer leads to the formation of an accretion disk. Tidal interactions between the disk and the donor star then allow at least some fraction of the angular momentum carried by the transferred matter to be returned to the orbit. However, if the size of the accretor is a considerable fraction of the size of the orbit, matter lost by the donor star through the inner Lagrangian point may impact the accretor's surface directly rather than form an accretion disk.

In this paper, we complement the work of Sepinsky et al. (2007b, hereafter Paper I) and Sepinsky et al. (2009) by investigating the orbital evolution due to mass overflow in eccentric binaries in which no disk forms around the accretor. For this purpose, we calculate the trajectories of mass elements escaping through the inner Lagrangian point of the donor star in the ballistic limit, and distinguish between three possible cases: (1) the ejected matter falls back onto the donor star, (2) the ejected matter impacts the surface of the accretor, and (3) the ejected matter orbits the accretor for at least one orbital revolution of the binary. In the first two cases, the evolution of the orbital elements is obtained directly from the ballistic trajectory calculations. In the third case, the evolution of the orbital elements depends on the interactions between mass elements ejected during successive periastron passages of the donor star. Since such interactions are

expected to violate our assumption of particles moving in the ballistic limit, we do not consider them here.

The present paper is organized as follows. In § 2, we outline the basic assumptions and methodology used to study ballistic particle trajectories and the effects of mass overflow on the orbital evolution of eccentric binaries. In § 3, we examine the fate of mass lost by the donor star as a function of the initial binary properties and identify ranges of initial parameters leading to fallback, direct impact accretion, and possible disk formation. Evolutionary sequences and timescales of orbital evolution due to mass overflow in eccentric binaries are presented in § 4. The final section, § 5, is devoted to concluding remarks.

2. MASS OVERFLOW IN ECCENTRIC BINARIES

2.1. *Basic assumptions*

We consider a close binary system of stars with masses M_1 and M_2, and spherical radii $\mathcal{R}_1$ and $\mathcal{R}_2$. We define the binary mass ratio as $q = M_1/M_2$, and assume the initial orbit to be Keplerian with semi-major axis a, eccentricity e, and orbital period $P_{\rm orb}$. The periastron distance of the two stars is then $r_P = a(1-e)$.

The binary component stars are assumed to rotate uniformly with rotational angular velocities $\vec{\Omega}_1$ and $\vec{\Omega}_2$ around axes perpendicular to the orbital plane and in the same sense as the orbital motion. For convenience, we express the rotational angular velocities in units of the orbital angular velocity $\vec{\Omega}_P$ at periastron:

$$\vec{\Omega}_1 = f_1\,\vec{\Omega}_P, \qquad \vec{\Omega}_2 = f_2\,\vec{\Omega}_P \tag{1}$$

with

$$|\vec{\Omega}_P| = \frac{(1+e)^{1/2}}{(1-e)^{3/2}}\,\frac{2\,\pi}{P_{\rm orb}}. \tag{2}$$

Hence, f_1 and f_2 are a dimensionless parameterization of the rotation rates of stars 1 and 2, respectively, in terms of $|\vec{\Omega}_P|$.

For stars in a circular synchronous binary orbit, it is commonly assumed that the surface of the star will conform to the equipotential surface which encloses the same volume as the spherical radius of the star. The maximum size of the star is then determined by the size of the Roche lobe, which is defined by the equipotential surface passing through the L_1 point. For eccentric binaries, we follow Sepinsky et al. (2007a,b) and construct effective equipotential surfaces using a reference frame corotating with the star such that the envelope is instantaneously quasi-static (see also Plavec 1958; Limber 1963; Avni 1976). For an analysis of the validity of this assumption, see Sepinsky et al. (2007a). In this reference frame we can locate the effective L_1 point at the minimum of the potential along the line connecting the mass centers of the two stars [1]. We can then identify the effective Roche lobe as the equipotential surface passing through this effective L_1 point.

At some point in time, one of the stars is assumed to fill its effective Roche lobe due to the expansion of the star and/or the contraction of the orbit. For brevity, we refer to the effective Roche lobe-filling star as star 1 and to its companion as star 2. Since the stars are in an eccentric orbit, the size of star 1's effective Roche lobe is a function of time and is smallest when the stars are at periastron (Sepinsky et al. 2007a, hereafter SWK). Roche lobe overflow is therefore expected to take place first at periastron and then re-occur at each subsequent periastron passage.

To model the episodic mass loss at successive periastron passages, we assume a small amount of mass M_3 ($M_3 \ll M_1, M_2$) to be ejected from star 1 through its inner Lagrangian point L_1 at each periastron passage. As in Paper I, we assume the mass overflow rate $\dot{M}_1$ from the star to be a Dirac delta function of amplitude $\dot{M}_0 < 0$ centered on the periastron of the binary orbit:

$$\dot{M}_1 = \dot{M}_0\,\delta(\nu) \tag{3}$$

where ν is the true anomaly with $\nu = 0$ at the periastron, and a normalization factor of $2\,\pi$ has been absorbed in the constant value for $\dot{M}_0$. The mass of the ejected particle is then related to the mass overflow rate $\dot{M}_0$ by

$$M_3 = \int_{-P_{\rm orb}/2}^{P_{\rm orb}/2} (-\dot{M}_1)\,dt = -\frac{(1-e)^{3/2}}{(1+e)^{1/2}}\,\frac{P_{\rm orb}}{2\pi}\,\dot{M}_0, \tag{4}$$

where we made use of the relation

$$dt = \frac{\left(1-e^2\right)^{3/2}}{\left(1+e\cos\nu\right)^2}\,\frac{P_{\rm orb}}{2\pi}\,d\nu. \tag{5}$$

In figure 1, we show the orbit for a system with initial eccentricity $e_i = 0.3$, initial donor rotation rate $f_{1,i} = 0.8$, and initial mass ratio $q_i = 2.0$ in a reference frame where star 2 is stationary. The ejected particle undergoes self-accretion, and its trajectory is shown by the dotted line. The orbit of the donor star is eccentric and shown by the short-dashed line. The position of star 2 is indicated by the point, and the dashed-dotted line shows its spherical radius. The donor star is shown at three positions (from right to left, respectively): periastron, particle impact, and apastron, and moves in the counter-clockwise direction. The spherical radius of the donor star, $\mathcal{R}_1$, is shown by the long-dashed line and is a constant radius for each of the positions shown. The effective Roche lobe of star 1 is also drawn at each position. It is clear that the effective Roche lobe radius of star 1 grows relative to its initial size as it moves away from periastron. We also indicate the true anomaly, ν, which measures the angle of the line connecting the mass centers of the stars in a Keplerian orbit measured counterclockwise from periastron.

Furthermore, we consider the particle to impact the surface of a star when it falls within the spherical radius of that star. This surface does not lie at the Roche lobe, as can be seen in Figure 1. Due to the computational complexity and time-variable shape of the effective Roche lobe, calculations of this kind were not considered here. If this calculation were included, it is clear that the particle would strike the surface of the effective Roche lobe earlier in the orbit. In fact, for many of the cases studied, the ejected particle never moves further from the donor star than the position of the L_1 point at periastron. Thus, for

[1] We note that viscosity in the stellar atmosphere will cause a tidal lag or lead in the position of L_1 with respect to line connecting the centers of the two stars, to a degree dependent on the asynchronism of the star. We intend to include tidal lags and leads in future investigations.

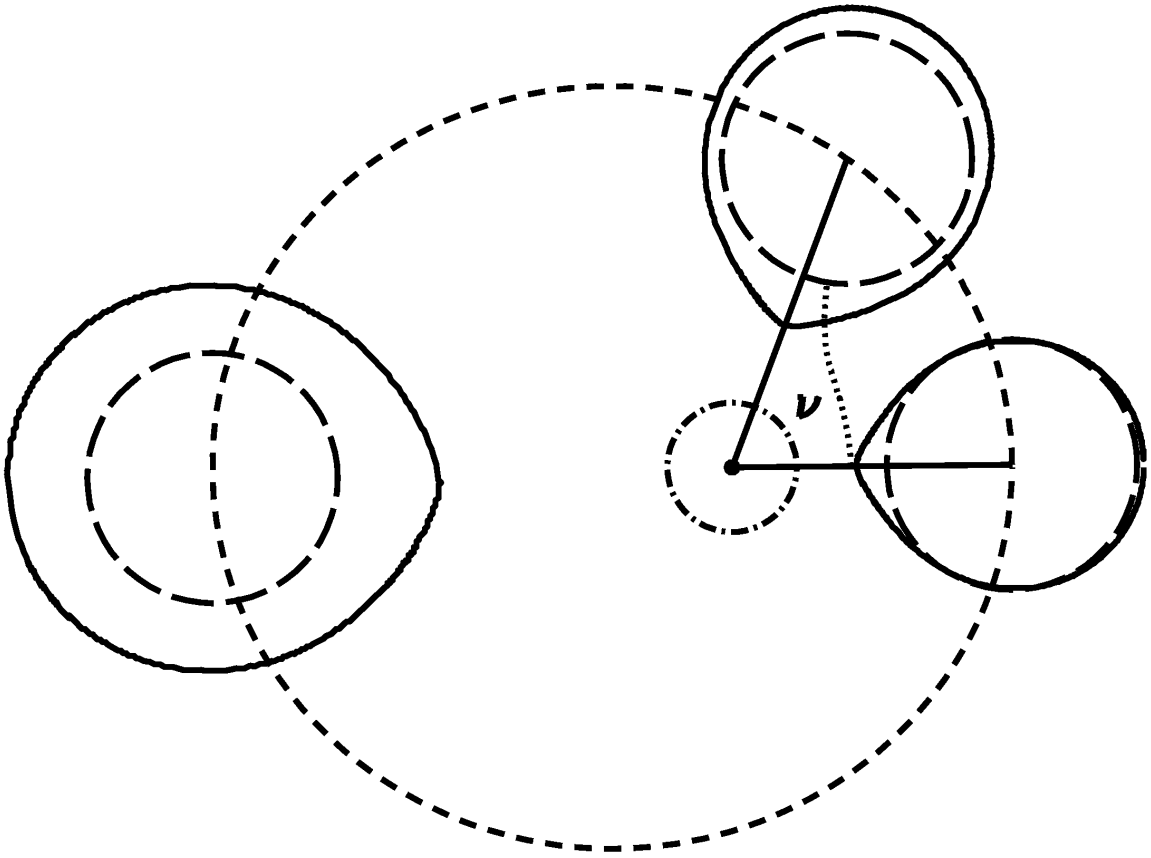

FIG. 1.— A schematic representation of the orbit of the donor star (short-dashed line) in a reference frame fixed to star 2. In this diagram, we show the constant radius of star 2 (dashed-dotted lines), the constant radius of the donor (long-dashed line), the time-dependent effective Roche lobe (solid line), and the path of the ejected particle (dotted line). The donor star is shown at three different positions in the orbit: periastron, particle impact, and apastron. The true anomaly, ν, is the angle of the line connecting the mass centers of the stars measured with respect to periastron, and is indicated above. For this orbit ($q_i = 2.0$, $f_{1,i} = 0.8$, $e_i = 0.3$), the ejected particle impacts the donor star at $\nu \simeq 1.21$ radians.

these cases, if we assumed impact occurred at the surface of the effective Roche lobe, no mass loss would occur at the L_1 point, and thus we would not expect any orbital evolution due to this effect. As such, it may be possible for non-synchronous, eccentric systems to effectively halt mass loss through the L_1 point. We will investigate this effect in a future study.

2.2. *Ballistic particle trajectories*

Our aim in this paper is to investigate the evolution of the orbital elements due to mass overflow in eccentric binaries. For this purpose, we treat the binary components as rigid spheres of uniform density. The matter ejected by the donor star at each periastron passage is treated as a point mass. To describe the motion of the stars and the ejected mass elements, we introduce an inertial frame of reference $OXYZ$ with origin O at the initial center of mass of the binary prior to any mass overflow, and with the XY-plane coinciding with the orbital plane. The orientation of the axes is chosen such that the positive direction of the X-axis coincides with the line from the binary mass center to the position of the donor star at the onset of mass overflow, and the positive Z-axis is parallel to the direction of the orbital angular momentum vector at the onset of mass overflow.

To determine whether a star undergoes mass overflow, its volume-equivalent Roche lobe radius is calculated accounting for the effects of eccentricity and non-synchronous rotation, as described in detail in SWK. Since we here do not consider the detailed structure of the donor star, we assume the matter ejected at periastron to have an initial velocity $\vec{V}_3$ equal to the vector sum of the star's rotational velocity at L_1 and its orbital velocity at periastron:

$$\vec{V}_3 = \vec{\Omega}_1 \times \vec{r}_{L_1} + \vec{V}_1. \tag{6}$$

Here, $\vec{r}_{L_1}$ is the vector from the center of mass of star 1 to the L_1 point, and $\vec{V}_1$ the orbital velocity of star 1 at periastron right before the ejection of the matter. We do not consider any contribution to $\vec{V}_3$ from the thermal speed of the mass elements in the donor's atmosphere (Lubow & Shu 1975). A generalization of our calculations accounting for the thermal speed is straightforward, but adds extra dimensions to the parameter space explored in this paper. We therefore defer this extension to a future investigation.

After the ejection of a mass element from the L_1 point, the system evolves as a three-body system according to the equations of motion

$$\frac{d^2\vec{R}_k}{dt^2} = -\sum_{\substack{j=1 \\ j\neq k}}^{3} \frac{G\,M_j}{|\vec{r}_{kj}|^2}\,\frac{\vec{r}_{kj}}{|\vec{r}_{kj}|} \qquad (k = 1, 2, 3), \tag{7}$$

where G is the Newtonian gravitational constant, $\vec{R}_1$ and $\vec{R}_2$ are the position vectors of star 1 and star 2 with respect to the inertial frame of reference, $\vec{R}_3$ is the position vector of the ejected mass element with respect to the inertial frame, and $\vec{r}_{kj} = \vec{R}_k - \vec{R}_j$.

For numerical convenience, we express equations (7) and the initial condition given by equation (6) in terms dimensionless quantities $\vec{R}_j^*$, M_j^*, t^*, $\vec{V}_j^*$, and $\vec{\Omega}_P^*$ defined as

$$\vec{R}_j^* = \vec{R}_j / r_{P,i}, \quad j = 1,2,3 \tag{8}$$

$$M_j^* = M_j / M_T, \quad j = 1,2,3 \tag{9}$$

$$\vec{V}_j^* = \vec{V}_j \sqrt{\frac{r_{P,i}}{GM_T}}, \quad j = 1,2,3 \tag{10}$$

$$t^* = t \sqrt{\frac{GM_T}{r_{P,i}^3}}, \tag{11}$$

$$\vec{\Omega}_P^* = \vec{\Omega}_P \sqrt{\frac{r_{P,i}^3}{GM_T}}, \tag{12}$$

where $r_{P,i}$ is the initial periastron distance between the binary components at the onset of mass overflow, M_T is the total system mass, and the subscripts $j = 1,2,3$ refer to star 1, star 2, and the ejected particle, respectively. In equation (6), we also express the position of the L_1 point in units of the initial periastron distance as

$$\vec{r}_{L_1}^* = \frac{\vec{r}_{L_1}}{r_{P,i}}. \tag{13}$$

The quantity $\vec{r}_{L_1}^*$ depends only on the binary mass ratio, the orbital eccentricity, the true anomaly, and the rotation rate of star 1 in units of the orbital angular velocity at periastron (See Equation [A15] of Paper 1).

In terms of these dimensionless quantities, the initial positions and velocities of the stars and ejected particle are

$$\vec{R}_{1,i}^* \equiv (X_{1,i}^*, Y_{1,i}^*, Z_{1,i}^*) = (\frac{1}{1+q_i}, 0, 0), \tag{14}$$

$$\vec{R}_{2,i}^* \equiv (X_{2,i}^*, Y_{2,i}^*, Z_{2,i}^*) = (-\frac{q_i}{1+q_i}, 0, 0), \tag{15}$$

$$\vec{R}_{3,i}^* = \vec{r}_{L_1,i}^* \tag{16}$$

$$\vec{V}_{1,i}^* = \vec{R}_{1,i}^* \times \vec{\Omega}_{P,i}^*, \tag{17}$$

$$\vec{V}_{2,i}^* = \vec{R}_{2,i}^* \times \vec{\Omega}_{P,i}^*, \tag{18}$$

$$\vec{V}_{3,i}^* = f_{1,i} \vec{\Omega}_{P,i}^* \times \vec{r}_{L_1,i}^* + \vec{R}_{1,i}^* \times \vec{\Omega}_{P,i}^*, \tag{19}$$

where the subscript "i" indicates that the quantity is to be considered at the time the particle is ejected, recalling that the particle is ejected at periastron. Furthermore, equation 7 becomes

$$\frac{d^2 \vec{R}_k^*}{d(t^*)^2} = - \sum_{\substack{j=1 \\ j \neq k}}^{3} \frac{M_j^*}{|\vec{r}_{kj}^*|^2} \frac{\vec{r}_{kj}^*}{|\vec{r}_{kj}^*|} \qquad (k = 1,2,3). \tag{20}$$

In this form, both the initial conditions and the equations of motion are independent of the initial size of the orbit.

We use an 8th order Runge Kutta ordinary differential equation solver (Galassi et al. 2006) to integrate equations (20) forward in time, starting from the first periastron passage at which matter is ejected by the donor. The three-body integration ends when (1) the ejected matter impacts star 2 ("direct impact accretion"); (2) the ejected matter falls back onto star 1 ("self-accretion"); or (3) the donor star has completed a full orbital revolution and a new matter element is ejected at the periastron of the binary orbit. After the accretion of the ejected matter onto star 1 or 2 in cases (1) and (2), equations (7) are integrated as a two-body problem by setting $M_3 = 0$.

In binaries with eccentric orbits, fallback onto the donor star (case 2) is facilitated by the increasing size of the effective Roche Lobe as the distance between the stars increases following periastron passage (See SWK). The actual outcome of the mass ejection, though, also depends on the initial velocity of the ejected matter. In the case where no accretion takes place within one orbital revolution (case 3), the system evolves as a four-body system until one of the ejected matter elements is accreted by star 1 or star 2, or until another mass element is ejected at the next periastron passage. The successive ejection of mass elements during subsequent periastron passages, possibly causing the mass transfer stream to interact with itself, will likely lead to the formation of an accretion disk around star 2. A detailed study of accretion disk formation will not be investigated here. We therefore restrict ourselves to identifying the regions of parameter space where this outcome is expected.

Some example trajectories of particles ejected from the L_1 point of star 1 at the periastron of the initial binary orbit are shown in Figure 2, for binaries with different initial mass ratios, donor rotation rates, and orbital eccentricities. The initial positions of the stars and the ejected matter are marked by asterisks, and the X^* and Y^* coordinates are expressed in units of the initial periastron distance. The motion of the stars is counterclockwise about the origin, and the numbered points on the orbits show the position of that object at different equally spaced values of the true anomaly. In all cases the radius of the donor star is set equal to the volume-equivalent radius of its effective Roche lobe at the periastron of the initial binary orbit (see SWK), and the mass of the ejected matter is determined by means of equation (4). We note that as long as $M_3 \ll M_1, M_2$, the ballistic trajectories are independent of the actual value of the mass of the ejected matter. For the presented trajectories, star 2 is assumed to be a point mass.

We note that the *shape* of the particle trajectories, and hence the outcome of the mass overflow, is independent of the size of the orbit. This is because the equations of motion and the initial positions and velocities are all independent of the size of the orbit (see equations [14]-[20]).

In panels (a), (c), and (e), the ejected particles fall back onto the donor star in less than half an orbit, while in panels (b), (d), and (f) the particles end up orbiting the donor's companion. Since the companion is assumed to be a point mass with zero radius, none of the displayed trajectories lead to direct impact accretion. In panel (d), direct impact would occur if the companion had a radius greater than 1.5% of the initial periastron distance. Comparison of panels (a) and (b) shows that

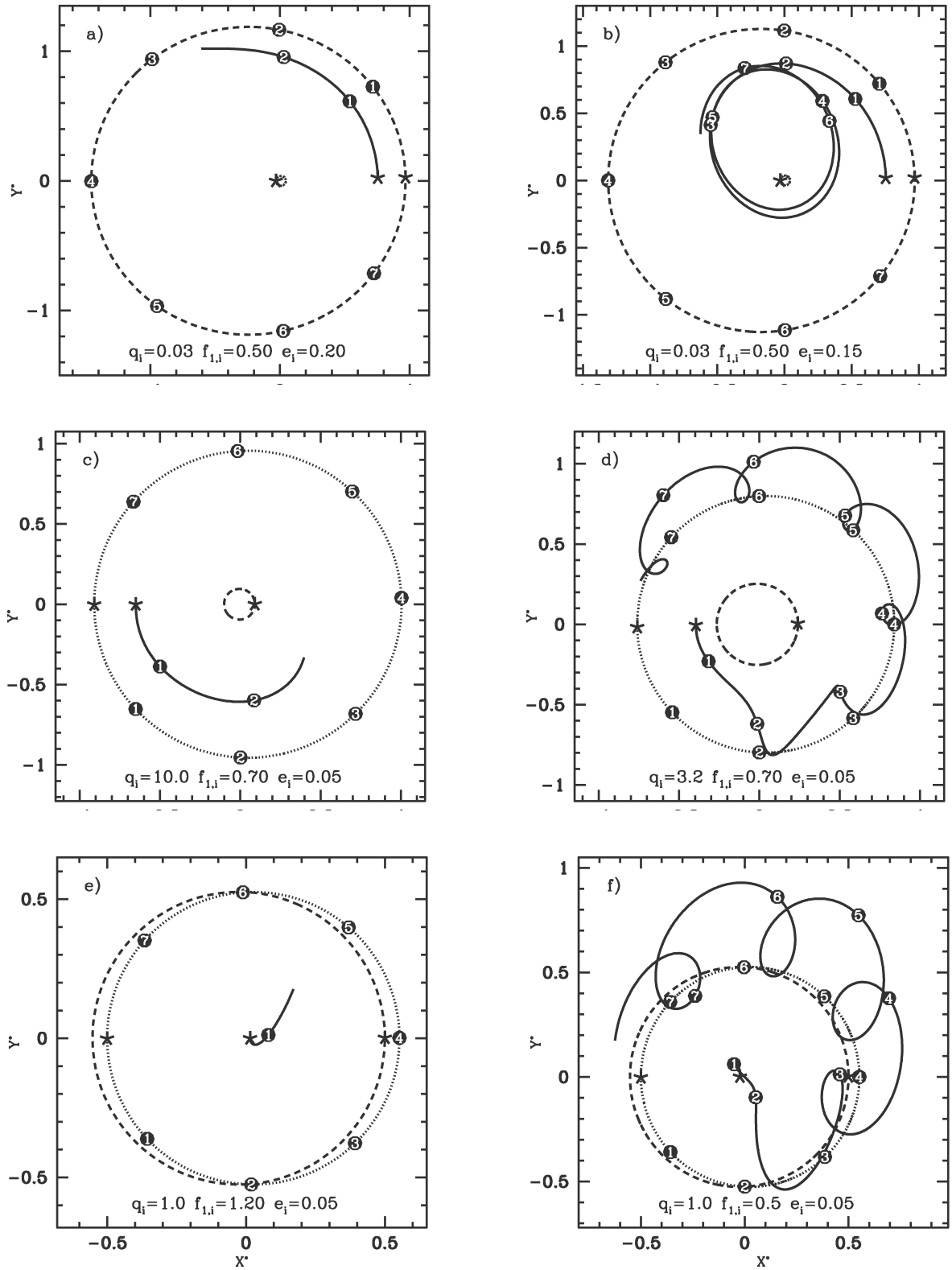

FIG. 2.— Example trajectories of particles ejected from the L_1 point in binaries with different initial mass ratios ($q_i = M_{1,i}/M_{2,i}$), donor rotation rates ($f_{1,i}$), and orbital eccentricities (e_i). The X^* and Y^* coordinates are Cartesian coordinates in the orbital plane expressed in units of the *initial* periastron separation between the two stars and with origin at the center of mass of the binary system. The solid lines represent the path of the ejected particle, the dashed lines the path of the donor star (star 1), and the dotted lines the path of the companion star (star 2), which is assumed to be a point mass. The motion of the stars and particles is counter-clockwise about the origin, starting from the asterisks indicating the initial position of the component stars and the ejected matter at the onset of Roche lobe overflow. The numbered points show the position of the stars and the ejected particle at seven different equally spaced values of the true anomaly. The orbits of the stars are drawn for one full orbit, regardless of whether the particle has accreted or not. In panels (a), (c), and (e), the particle paths are shown up until the point where the particle is accreted back onto the donor star. In panels (b), (d), and (f), the particles undergo neither direct impact nor self-accretion. The paths of the particles are therefore shown for one complete binary orbit.

small changes in the orbital eccentricity can significantly affect the type and outcome of the particle trajectories. In this particular case, the slightly smaller initial velocity of the ejected particle due to the lower eccentricity orbit in panel (b) is enough to cause the particle to fall towards star 2 rather than fall back onto star 1. Comparison of panels (c) and (d) as well as panels (e) and (f) shows that similar transitions in the behavior of the particle trajectories can be obtained by changing the initial binary mass ratio or the initial donor rotation rate.

2.3. *Spin evolution*

Since the initial velocity of the matter ejected at periastron depends on the rotation of the donor star, it is important to keep track of changes in the star's rotational angular velocity due to mass loss and accretion. To calculate the change in the rotational angular velocity of the donor star due to the loss of an element of mass M_3, we note that the total angular momentum $\vec{\mathcal{L}}_I$ in the system right before the ejection of matter at periastron is given by

$$\begin{aligned}\vec{\mathcal{L}}_I = & I_{1,I}\vec{\Omega}_{1,I} + I_{2,I}\vec{\Omega}_{2,I} \\ & + M_{1,I}\vec{R}_{1,I} \times \vec{V}_{1,I} + M_{2,I}\vec{R}_{2,I} \times \vec{V}_{2,I}, \end{aligned} \quad (21)$$

where I_1 and I_2 are the moments of inertia, $\vec{R}_1$ and $\vec{R}_2$ the position vectors, and $\vec{V}_1$ and $\vec{V}_2$ the velocities of star 1 and star 2, respectively, measured with respect to the inertial frame of reference. The subscript "I" denotes that the quantities are to be considered right before the ejection of matter at periastron. Similarly, the total angular momentum $\vec{\mathcal{L}}_F$ in the system right after the ejection of matter at periastron is given by

$$\begin{aligned}\vec{\mathcal{L}}_F = & I_{1,F}\vec{\Omega}_{1,F} + I_{2,F}\vec{\Omega}_{2,F} \\ & + M_{1,F}\vec{R}_{1,F} \times \vec{V}_{1,F} + M_{2,F}\vec{R}_{2,F} \times \vec{V}_{2,F} \\ & + M_3\vec{R}_3 \times \vec{V}_3, \end{aligned} \quad (22)$$

where $\vec{R}_3$ and $\vec{V}_3$ are the position and velocity vectors of the ejected mass element at the time of ejection measured with respect to the inertial frame of reference. The subscript "F" denotes that the quantities are to be considered right after the ejection of matter at periastron. For the uniform density spheres considered here, the moment of inertia is $I = 0.4M\mathcal{R}^2$. For a more centrally condensed object the moment of inertia will decrease, reducing the contribution of the spin to the total angular momentum.

Since the ejection of matter by star 1 does not instantaneously affect the companion star, all quantities pertaining to star 2 are identical right before and right after the instantaneous ejection of a mass element. Conservation of total angular momentum therefore yields

$$\begin{aligned}\vec{\Omega}_{1,F} = & \frac{1}{I_{I,F}}\Big(I_{1,I}\vec{\Omega}_{1,I} + M_{1,I}\vec{R}_{1,I} \times \vec{V}_{1,I} \\ & - M_{1,F}\vec{R}_{1,F} \times \vec{V}_{1,F} - M_3\vec{R}_3 \times \vec{V}_3\Big). \end{aligned} \quad (23)$$

In this equation, all quantities on the right-hand side are readily obtained from the initial conditions and the adopted mass overflow rate, except for $\vec{R}_{1,F}$ and $\vec{V}_{1,F}$. To determine $\vec{R}_{1,F}$ we assume M_3 is ejected perfectly inelastically, i.e., with no loss of linear momentum[2]. Furthermore, since the ejection is instantaneous, the center of mass of star 1 before the ejection is identical to the center of mass of the system consisting of the particle and star 1 after the ejection. Thus, the final position of star 1 is given by

$$\vec{R}_{1,F} = \frac{1}{M_{1,F}}\left(M_{1,I}\vec{R}_{1,I} - M_3\vec{R}_3\right). \quad (24)$$

The velocity $\vec{V}_{1,F}$ is determined from the conservation of linear momentum:

$$\vec{V}_{1,F} = \frac{1}{M_{1,F}}\left(M_{1,I}\vec{V}_{1,I} - M_3\vec{V}_3\right). \quad (25)$$

To calculate the change in the rotational angular velocity due to the fallback of the ejected matter onto the donor star, it suffices to replace M_3 by $-M_3$, and $\vec{R}_3$ and $\vec{V}_3$ by the position and velocity vector of the ejected mass element at the time of accretion in equations (23)–(25).

The change in the rotational angular velocity of star 2 due to direct impact accretion is derived similarly:

$$\begin{aligned}\vec{\Omega}_{2,F} = & \frac{1}{I_{2,F}}\Big[I_{2,I}\vec{\Omega}_{2,I} + M_{2,I}\vec{R}_{2,I} \times \vec{V}_{2,I} \\ & + M_3\vec{R}_3 \times \vec{V}_3 - M_{2,F}\vec{R}_{2,F} \times \vec{V}_{2,F}\Big] \end{aligned} \quad (26)$$

with

$$\vec{R}_{2,F} = \frac{1}{M_{2,F}}\left(M_{2,I}\vec{R}_{2,I} + M_3\vec{R}_3\right), \quad (27)$$

and

$$\vec{V}_{2,F} = \frac{1}{M_{2,F}}\left(M_{2,I}\vec{V}_{2,I} + M_3\vec{V}_3\right). \quad (28)$$

Here, the subscripts "I" and "F" denote the quantities are to be considered right before and right after the accretion of matter, respectively, and $\vec{R}_3$ and $\vec{V}_3$ are the position and velocity vector of the ejected mass element at the time of accretion.

2.4. *Calculation of the Orbital Elements*

Due to the gravitational interactions between the ejected matter and the component stars of the binary system, the orbital motion of the stars is no longer purely Keplerian. In particular, the semi-major axis and eccentricity are not constant in time. We calculate the instantaneous value of the osculating orbital elements of the binary system at each timestep using (Sterne 1960)

$$e^2 = 1 - \frac{\left|\vec{r}_{\rm rel} \times \vec{v}_{\rm rel}\right|^2}{G\left(M_1 + M_2\right)a}, \quad (29)$$

$$\frac{1}{a} = \frac{2}{|\vec{r}_{\rm rel}|} - \frac{v_{\rm rel}^2}{G\left(M_1 + M_2\right)}, \quad (30)$$

[2] We note that, in a perfectly inelastic collision energy is not conserved. We assume the existence of some mechanism, either internal or external, which allows the ejected particle to become physically separate from the donor star. Similarly for accretion, some process must exist to allow the particle and accretor to physically merge. In either case, the change in the total energy of the system is likely to happen at the expense of the thermal energy of the component stars. For further discussion of the change in the total energy, see §4.2

where $\vec{r}_{\rm rel}$ and $\vec{v}_{\rm rel}$ are, respectively, the position and velocity vectors of star 2 with respect to star 1. The osculating orbital elements represent the value of a and e that the orbit would have if the perturbative forces were removed at that instant. To keep track of changes in the position of the periastron due to mass overflow, we also calculate the instantaneous true anomaly of the binary system from

$$\cos\nu = \frac{1}{e}\left[\frac{a\left(1-e^2\right)}{|\vec{r}_{\rm rel}|} - 1\right]. \quad (31)$$

3. PARAMETER SPACE FOR DIRECT IMPACT AND SELF-ACCRETION

In order to investigate the parameter space leading to different outcomes of mass overflow (direct impact accretion, self-accretion, or possible disk formation) in binaries with eccentric orbits, we performed an extensive set of ballistic orbit calculations for binaries with different initial mass ratios q_i, initial donor rotation rates $f_{1,i}$, and initial orbital eccentricities e_i at the onset of mass overflow. As in §2.2, we set the donor's radius equal to the volume equivalent radius of its effective Roche lobe at the periastron of the initial binary orbit. We recall that as long as $M_3 \ll M_1, M_2$ the problem is fully determined by q_i, $f_{1,i}$, and e_i, and is independent of the actual values of the mass overflow rate $\dot{M}_0$, donor mass M_1, donor radius, $\mathcal{R}_1$, and initial orbital semi-major axis a_i. Star 2 is again treated as a point mass.

For each initial orbital eccentricity and donor rotation rate, we find a critical mass ratio, $q_{\rm crit}$, such that for $q_i > q_{\rm crit}$ the system undergoes self-accretion, while for $q_i < q_{\rm crit}$, the system may undergo direct impact accretion or form an accretion disk, depending on the radius of star 2. The critical mass ratio is shown in Figure 3 as a function of the donor's initial rotation rate for initial orbital eccentricities ranging from 0.01 to 0.2. In this eccentricity range, $q_{\rm crit}$ decreases with increasing initial orbital eccentricity, increasing the parameter space leading to self-accretion.

For initial eccentricities $e_i > 0.2$, mass overflow always leads to self-accretion if the initial binary mass ratio $q_i > 0.006$. In high-eccentricity systems direct impact accretion therefore only occurs for very low mass ratios. For initial donor rotation rates in the range $1.0 \le f_{1,i} \le 1.2$, mass ejection at periastron results in self-accretion for all initial mass ratios $10^{-3} < q_i < 10^3$, independent of the initial orbital eccentricity. For the purpose of this paper, we did not thoroughly explore the parameter space for $f_{1,i} > 1.2$, though calculation of some sample trajectories of mass ejected from highly super-synchronously rotating donor stars indicates the matter may start orbiting the donor star before leading to self-accretion.

When $q_i < q_{\rm crit}$, depending on the accretor's radius $\mathcal{R}_2$ the ejected matter can directly impact the companion star or go into orbit around it, possibly forming an accretion disk. While studying disk formation is beyond the capabilities of our ballistic trajectory code, we can investigate when direct impact rather than disk formation is expected to occur based on the ballistic trajectories of the ejected mass elements. For this purpose, we treat star 2 as a point mass and determine the minimum distance $r_{\rm min}$ between the ejected matter and star 2 during a single orbit for ballistic trajectories not leading to self-accretion. Hence, if $\mathcal{R}_2 > r_{\rm min}$, direct impact occurs within one binary orbital period. If $\mathcal{R}_2 < r_{\rm min}$, the ejected matter may still impact star 2 after one orbital period, but it may also orbit star 2 until it interacts with other ejected mass elements and forms an accretion disk.

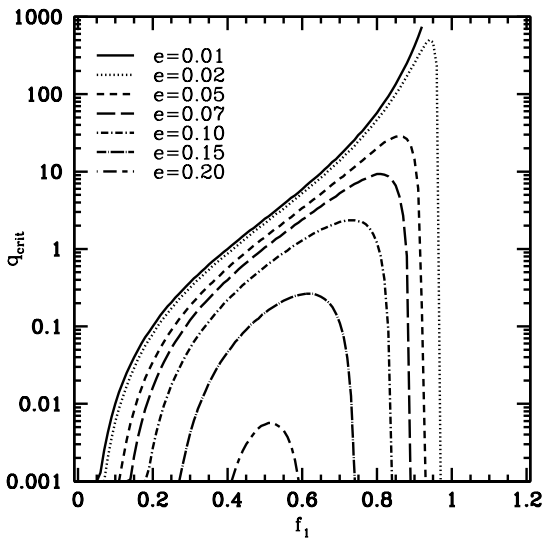

FIG. 3.— The critical mass ratio $q_{\rm crit}$ above which systems undergo self-accretion as a function of the donor's initial rotation rate $f_{1,i}$, for initial orbital eccentricities ranging from 0.01 to 0.2. For $q_i > q_{\rm crit}$, systems undergo self-accretion, while for $q_i < q_{\rm crit}$ systems undergo direct impact accretion or form an accretion disk, depending on the radius of the accretor. We note that for low initial eccentricities, $e_i \lesssim 0.05$, the delta-function approximation of the mass overflow rate given by equation (3) likely breaks down, so that at low eccentricities disk formation or direct impact may occur for a larger region of parameter space than presented here.

The minimum distance $r_{\rm min}/r_{P,i}$ is shown in Figure 4 as a function of the logarithm of the initial binary mass ratio q_i. For each initial mass ratio, the grey dots represent the minimum distance associated with different initial donor rotation rates ($0.01 \le f_{1,i} \le 1.0$) and initial orbital eccentricities ($0.01 \le e_i \le 0.2$). The main trend of $r_{\rm min}/r_{P,i}$ as a function of q_i is to decrease with increasing values of q_i. This is partly because the Roche lobe of star 2 is smaller for large mass ratios than for small mass ratios, or, equivalently, the initial position of the ejected matter, the L_1 point of star 1, is relatively closer to star 2 for large mass ratios than for small mass ratios (see SWK).

The lower and upper edges of the grey dotted region in Figure 4 can be approximated by

$$\frac{r_{\rm min,lower}}{r_{P,i}} = \exp\left[-0.16(\log_{10} q_i + 4.8)^2 - 0.13\right], \quad (32)$$

and

$$\frac{r_{\rm min,upper}}{r_{P,i}} = \exp\left[-0.1(\log_{10} q_i + 4.8)^2\right] - 0.01\log_{10} q_i + 0.05. \quad (33)$$

Hence, if $\mathcal{R}_2 > r_{\rm min,upper}$, the system always undergoes direct impact accretion within one orbital period. If $\mathcal{R}_2 < r_{\rm min,lower}$, the ejected matter always avoids impacting the donor's companion star within one orbital period, so that an accretion disk may be formed. If $r_{\rm min,lower} < \mathcal{R}_2 < r_{\rm min,upper}$, the outcome of the mass

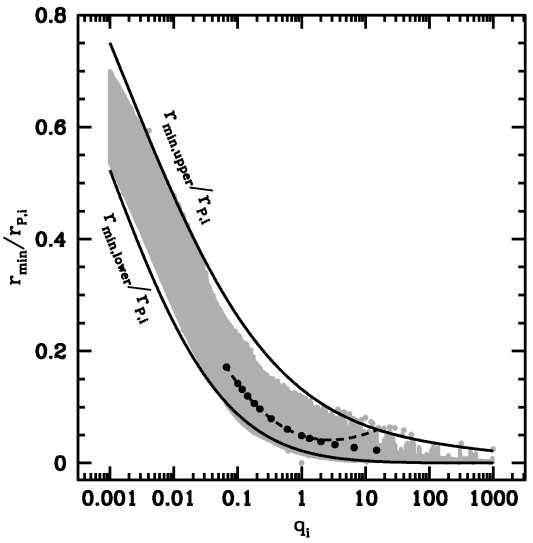

FIG. 4.— The minimum distance $r_{\rm min}/r_{P,i}$ from star 2 (assumed to be a point mass) reached by matter ejected from the L_1 point of the donor star at the periastron of the binary orbit as a function of the logarithm of the initial binary mass ratio q_i. The distance is measured in the orbital plane and is normalized to the initial periastron separation $r_{P,i}$ between the two stars. For a given mass ratio, the grey dots represent minimum distances for different initial donor rotation rates $f_{1,i}$ ranging from 0.01 to 1.0, and initial orbital eccentricities e_i ranging from 0.01 to 0.2. The solid lines represent the approximate upper and lower limits on the minimum distance as a function of q_i given by equations (32) and (33). The black circles are the data of Lubow & Shu (1975) for the closest approach of a ballistic particle in a circular, synchronous binary system, and the dashed line is the fit to the data of Lubow & Shu (1975) given by Nelemans et al. (2001). Both the fit and the data shown are adjusted to account for the different definitions of the mass ratio given in those papers.

overflow depends on the initial donor rotation rate and orbital eccentricity.

For comparison, the black circles of Figure 4 show the distance of closest approach for a particle in a circular, synchronous binary system as calculated by Lubow & Shu (1975) (their $\varpi_{\rm min}$), where we have taken into account the difference between their and our definition of the mass ratio. We note that this data is consistent with our calculation of the distance of closest approach, and that the inclusion of non-synchronous rotation and/or eccentricity can either increase or decrease the distance of closest approach. The dashed line through these data points is the fit to the data of Lubow & Shu (1975) given by Nelemans et al. (2001). The fit is very accurate for $q_i \lesssim 2$, but should not be extrapolated to large q_i. This does not affect the results of Nelemans et al. (2001), as they are interested in double white dwarf systems where the mass ratio of the system is generally less than unity.

4. ORBITAL EVOLUTION DUE TO MASS OVERFLOW

Using the framework described in §2, we can now investigate the secular evolution of the orbital elements due to the effects of mass overflow in eccentric binary systems. Combining equations (23)–(28) with equations (29)–(31), it can be seen that the changes in the orbital elements, and thus the time scales of orbital evolution, depend on the binary component masses, the donor radius and rotation rate (through the initial particle velocity), and the orbital elements (also through the initial particle velocity). The outcome of the mass overflow (e.g. whether or not direct impact accretion occurs) also depends on the radius of the accretor.

Once mass overflow starts, the radius of the donor star evolves due to the combined effects of mass loss and stellar evolution. In addition, the radius of the donor's effective Roche lobe changes due the evolution of its rotational angular velocity, the orbital elements, and the binary mass ratio (SWK). In order for mass overflow in eccentric binaries to be stable and long-lived, the radial evolution of the donor star must follow the evolution of its effective Roche lobe at the periastron of the binary orbit. In this section, we explore the potential long-term evolution of effective Roche lobe overflowing binaries with eccentric orbits, *assuming* that after the onset of mass overflow the donor star's radius remains equal to the radius of its effective Roche lobe at each subsequent periastron passage. Whether the response of the star to mass loss renders this possible depends on its internal structure and on the binary properties. Since we here treat the stars as rigid spheres, we defer questions on the longevity and the stability of mass overflow to future investigations.

To illustrate the effects of mass overflow in eccentric binaries, we consider a binary star system consisting of two rigid spheres with radii representative of main-sequence stars. The first rigid sphere ("star 1") is assumed to have a radius representative of a star near the end of core-hydrogen burning when the main-sequence radius is maximal, while the second rigid sphere ("star 2") is assumed to be a zero-age main-sequence star. Such a binary consisting of two non-coeval component stars can be formed through dynamical interactions in globular clusters. The adopted configuration allows us to illustrate the orbital evolution time scales of binaries with initial mass ratios $q_i < 1$ as well as binaries with initial mass ratios $q_i > 1$. In addition, a zero-age main-sequence accretor constitutes a big enough "target" to provide a non-negligible parameter space leading to direct impact accretion. A study of direct impact accretion in compact object binaries, double white dwarfs in particular, will be presented in a forthcoming paper.

4.1. *Orbital Evolution Timescales*

In Figures 5 – 8, we show the variations of the instantaneous characteristic timescales $\tau_a = |a/\dot{a}|$ for the evolution of the orbital semi-major axis a and $\tau_e = |e/\dot{e}|$ for the evolution of the orbital eccentricity e, as contour plots in the (q_i, e_i)-plane at the start of mass overflow. The considered range of initial mass ratios is $0.01 \leq q_i \leq 100$. Each panel in the figures corresponds to different values of the initial donor mass $M_{1,i}$ and the initial rotation rate $f_{1,i}$. The mass overflow rate at periastron is taken to be $\dot{M}_0 = -10^{-9}\, M_\odot\, {\rm yr}^{-1}$. Since the resulting timescales are inversely proportional to $\dot{M}_0$, the results can easily be rescaled to different mass overflow rates. The radii of the two stars are calculated using the analytic formulae for stellar evolution derived by Hurley et al. (2000).

To calculate the instantaneous rates of secular evolution of the orbital elements, we follow the evolution of the orbital semi-major axis and eccentricity of eccentric, effective Roche lobe overflowing binaries for 100 consecutive orbits. During this evolution, transitions may take

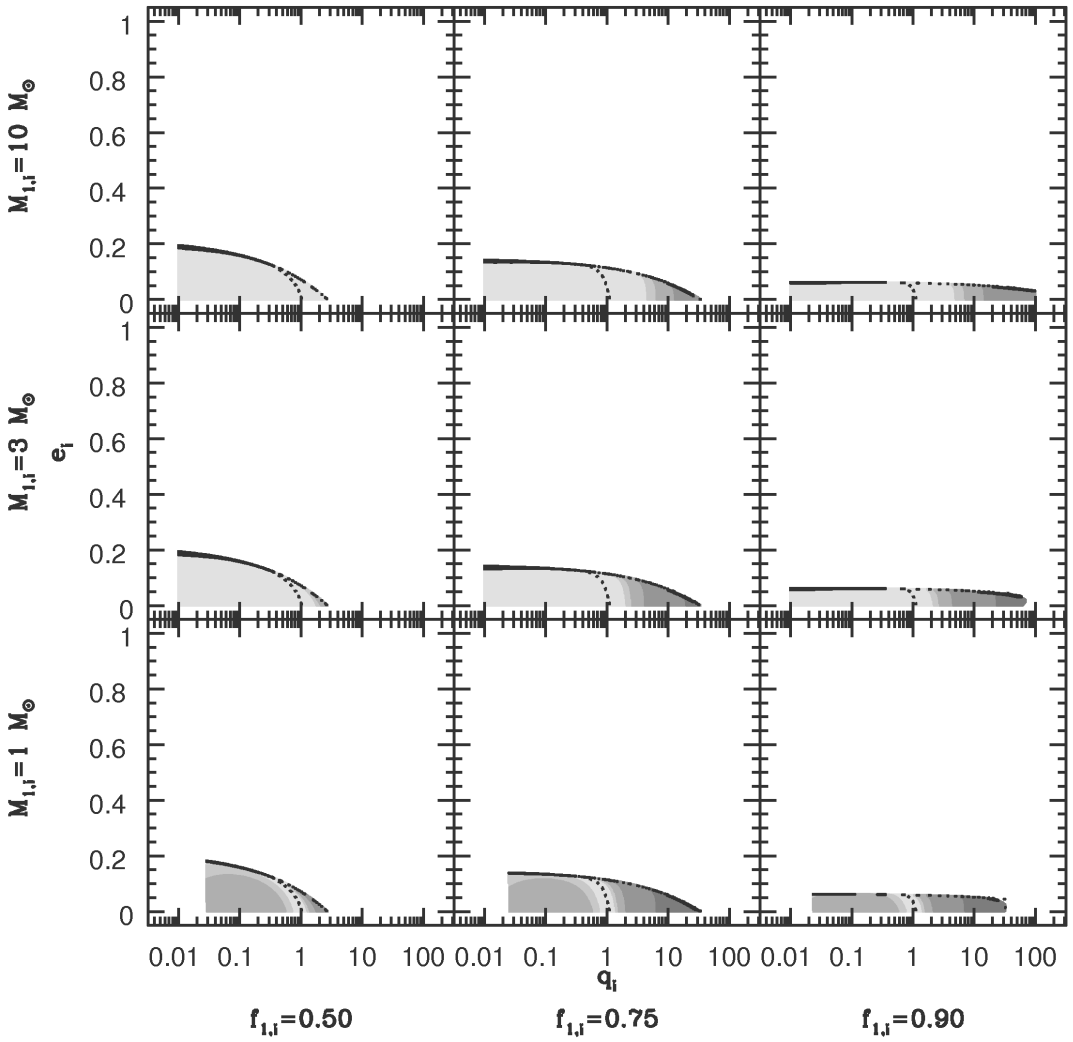

FIG. 5.— Timescales for the evolution of the semi-major axis a as a function of the initial mass ratio q_i and initial orbital eccentricity e_i in systems undergoing direct impact accretion. The donor star is assumed to be near the end of the main sequence and to have an initial mass $M_{1,i} = 1, 3$, or $10\,M_\odot$, and an initial rotation rate $f_{1,i} = 0.5, 0.75$, or 0.9. The accretor is assumed to be a zero-age main-sequence star with a mass determined by the initial mass ratio q_i. The mass overflow rate $\dot{M}_0$ at periastron is $-10^{-9}\,M_\odot\,\mathrm{yr}^{-1}$. The different shades of gray represent regions in the (q_i, e_i) parameter space with different characteristic timescales of orbital evolution. From the darkest to the lightest shade of gray, the timescales are: $0\,\mathrm{Gyr} < |\tau_a| < 1\,\mathrm{Gyr}$, $1\,\mathrm{Gyr} < |\tau_a| < 5\,\mathrm{Gyr}$, $5\,\mathrm{Gyr} < |\tau_a| < 10\,\mathrm{Gyr}$, $10\,\mathrm{Gyr} < |\tau_a| < 15\,\mathrm{Gyr}$, $15\,\mathrm{Gyr} < |\tau_a|$. The dotted black line near $q_i = 1$ divides the regions of the (q_i, e_i) parameter space where the semi-major axis increases as a function of time (to the left of the line) from the regions of the (q_i, e_i) parameter space where the semi-major axis decreases as a function of time (to the right of the line). The black shaded area corresponds to regions of the parameter space where the mode of mass overflow switches from direct impact to self-accretion or possible disk formation within the first 100 orbits after the onset of mass overflow. This area occupies only a small space between the the direct impact and self-accretion regimes. Unshaded regions correspond to regions of the parameter space where mass overflow either does not lead to direct impact accretion or the zero-age main-sequence accretor is so large that a contact binary rather than a semi-detached binary is formed.

place from direct impact accretion to self-accretion or vice versa. Systems for which this happens within 100 orbits from the start of mass overflow are confined to a fairly restricted region of the parameter space and are shown in black in Figures 5–8. In addition, for small initial mass ratios $q_i \lesssim 0.01 - 0.02$, the radius of star 2 is so large relative to the size of the orbit that the binary becomes a contact binary rather than a semi-detached binary. These binaries are also left out of consideration in Figures 5–8. For binaries that do not transition between direct impact and self-accretion and that do not form contact binaries, timescales of orbital evolution are calculated by averaging the changes in the orbital elements over one orbital period.

Figures 5 and 6 show the orbital evolution timescales for the semi-major axis and eccentricity for the case of direct impact accretion. The dotted line in the figures separates regions of the parameter space where a and e increase (to the left of the dotted line) from regions of the parameter space where a and e decrease (to the right of the dotted line). For small orbital eccentricities, the transition from increasing to decreasing orbital semi-

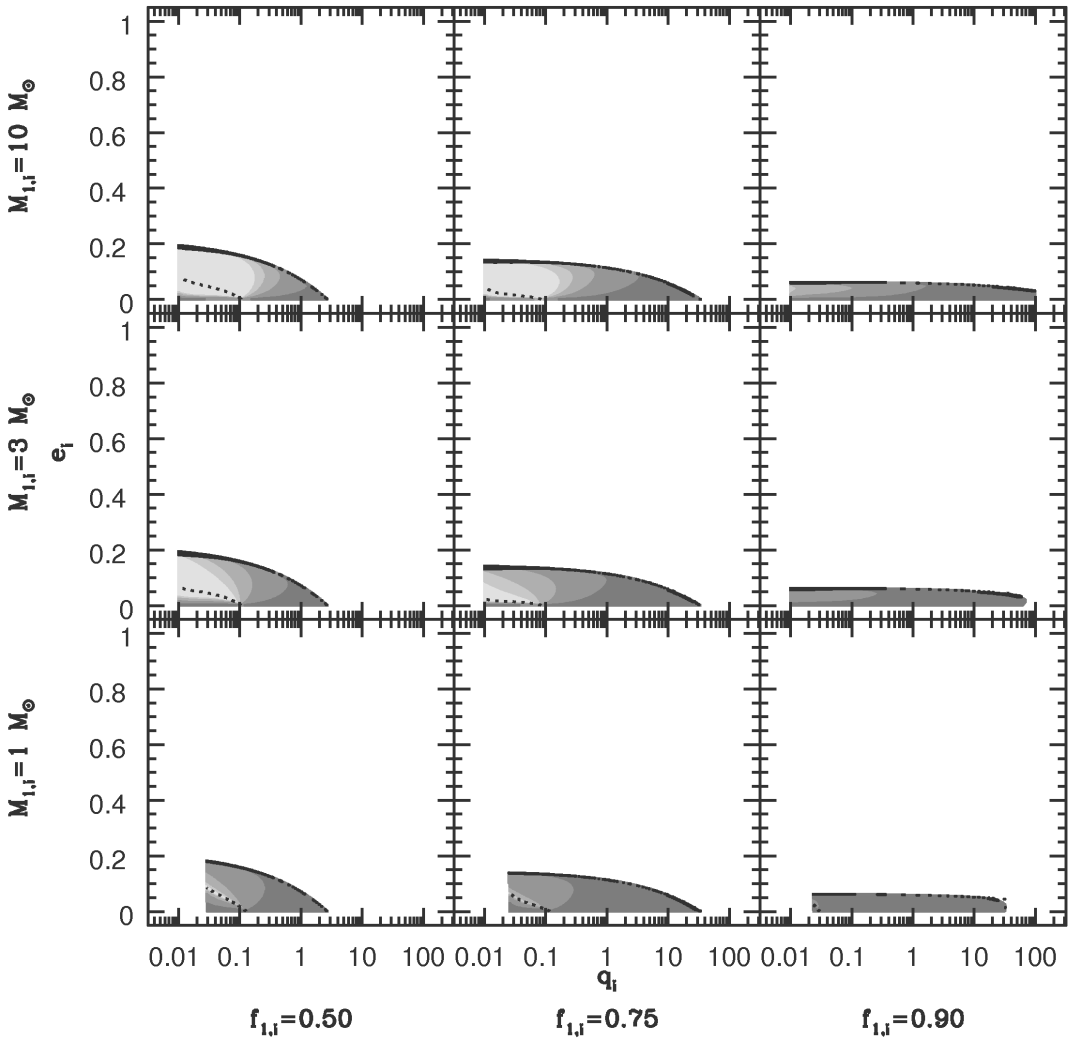

FIG. 6.— Same as Figure 5, but for the evolution of the orbital eccentricity e.

major axis occurs near $q_i = 1$, consistent with what is expected for conservative mass transfer in binaries with circular orbits (see, e.g., Paper I). As the eccentricity increases, the dividing line between increasing and decreasing semi-major axis moves toward smaller q_i. For a given choice of binary parameters, the orbital eccentricity typically evolves on shorter timescales than the orbital semi-major axis. The eccentricity evolution furthermore tends to circularize the orbit on fairly short timescales for most of the explored parameter space. Eccentricity pumping is only found for low initial binary mass ratios ($q_i \lesssim 0.1$), low initial orbital eccentricities ($e_i \lesssim 0.05$), and substantially subsynchronous rotation ($f_{1,i} \lesssim 0.75$).

Figures 7 and 8, show the orbital evolution timescales for the orbital semi-major axis and eccentricity in the case of self-accretion. Unlike the direct impact case, self-accretion always acts to decrease both the semi-major axis a and the orbital eccentricity e. The evolution of both a and e is furthermore fastest for larger binary mass ratios and lower orbital eccentricities. Comparison of Figures 7 and 8 with Figures 5 and 6 furthermore shows that the contours for self-accretion systems complement those for direct impact systems.

4.2. *Example Orbital Evolution Sequences*

In Figures 9 and 10 we show the long-term evolution of orbital and stellar properties for a representative sample of systems undergoing direct impact and self-accretion, respectively, for a mass overflow rate of $\dot{M}_0 = -10^{-9}\, M_\odot\, \mathrm{yr}^{-1}$. Following the procedure outlined in §2, a particle is ejected from the donor star at each periastron passage of the binary, and its ballistic orbit is followed until direct impact or self-accretion occurs. Impact of the particle on either star is determined under the assumption that the star is spherically symmetric and uniform in density ($I = 0.4 M \mathcal{R}^2$). Hence, we do not account for deviations from spherical symmetry due to rotation and tidal interactions.

Following the accretion of the particle, the system evolves as a two body system until it reaches the pe-

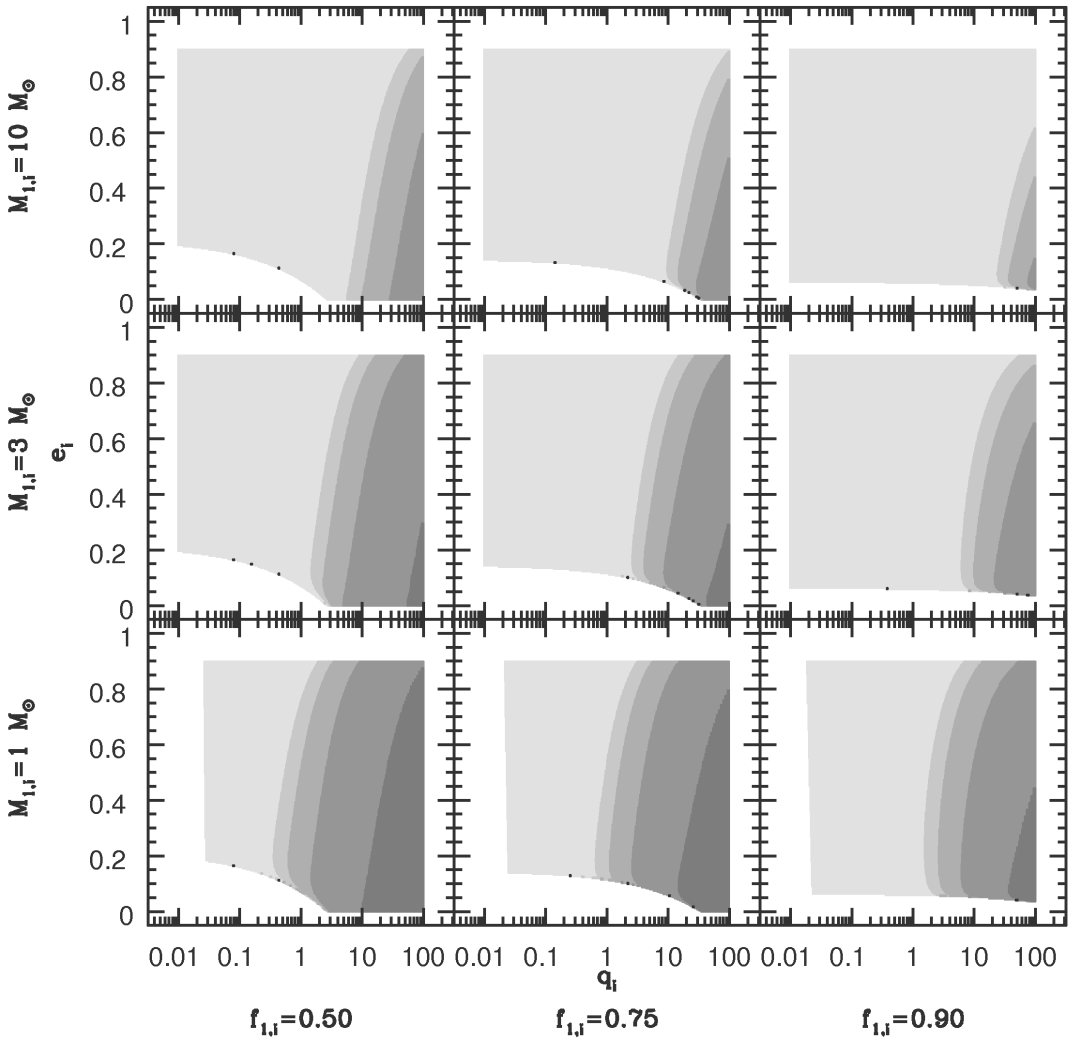

FIG. 7.— Timescales for the evolution of the semi-major axis a as a function of the initial mass ratio q_i and initial orbital eccentricity e_i in systems undergoing self-accretion. The donor star is assumed to be near the end of the main sequence and to have an initial mass $M_{1,i} = 1, 3$, or $10\,M_\odot$, and an initial rotation rate $f_{1,i} = 0.5, 0.75$, or 0.9. The binary companion is assumed to be a zero-age main-sequence star with a mass determined by the mass ratio q_i. The mass overflow rate at periastron is $\dot{M}_0 = -10^{-9}\,M_\odot\,\mathrm{yr}^{-1}$. The different shades of gray represent regions in the (q_i, e_i) parameter space with different characteristic timescales of orbital evolution. From the darkest to the lightest shade of gray, the timescales are: $0\,\mathrm{Gyr} < |\tau_a| < 1\,\mathrm{Gyr}$, $1\,\mathrm{Gyr} < |\tau_a| < 5\,\mathrm{Gyr}$, $5\,\mathrm{Gyr} < |\tau_a| < 10\,\mathrm{Gyr}$, $10\,\mathrm{Gyr} < |\tau_a| < 15\,\mathrm{Gyr}$, $15\,\mathrm{Gyr} < |\tau_a|$. The timescales always represent a decrease of the semi-major axis. The black points at low eccentricity correspond to regions of the parameter space where the mode of mass overflow switches from self-accretion to direct impact accretion or possible disk formation within the first 100 orbits after the onset of mass overflow. These points occupy only a small space between the the direct impact and self-accretion regimes. Unshaded regions correspond to regions of the parameter space where either mass overflow does not lead to self-accretion or the zero-age main-sequence accretor is so large that a contact binary rather than a semi-detached binary is formed.

riastron of the new orbit. At this point, the effective Roche lobe radius will also have changed compared to its value at the time of the previous mass ejection due to changes in the binary mass ratio, semi-major axis, eccentricity, and donor rotation rate. Since we assume the radius of the donor star to remain equal to the radius of its effective Roche lobe at periastron during the lifetime of the mass overflow phase, the donor rotation rate must be updated in accordance with conservation of spin angular momentum before the next mass ejection at periastron. Because the donor rotation rate in turn affects the radius of the effective Roche lobe, a root-finding algorithm is used to calculate a new self-consistent radius and rotation rate for the donor star immediately before the ejection of matter at each consecutive periastron passage. Throughout our numerical integrations, the total angular momentum of the system (defined as the spin angular momenta of stars 1 and 2 plus the orbital angular momentum of the system), is conserved to within a factor of 10^{-7}.

In Figures 9 and 10, the fractional changes of the donor radius $\mathcal{R}_1$, total energy, $E_{\rm tot}$, eccentricity, e, semi-major axis, a, spin orbital angular momentum of stars 1 and 2, J_{s1} and J_{s2}, and the rotation rates of stars 1 and 2,

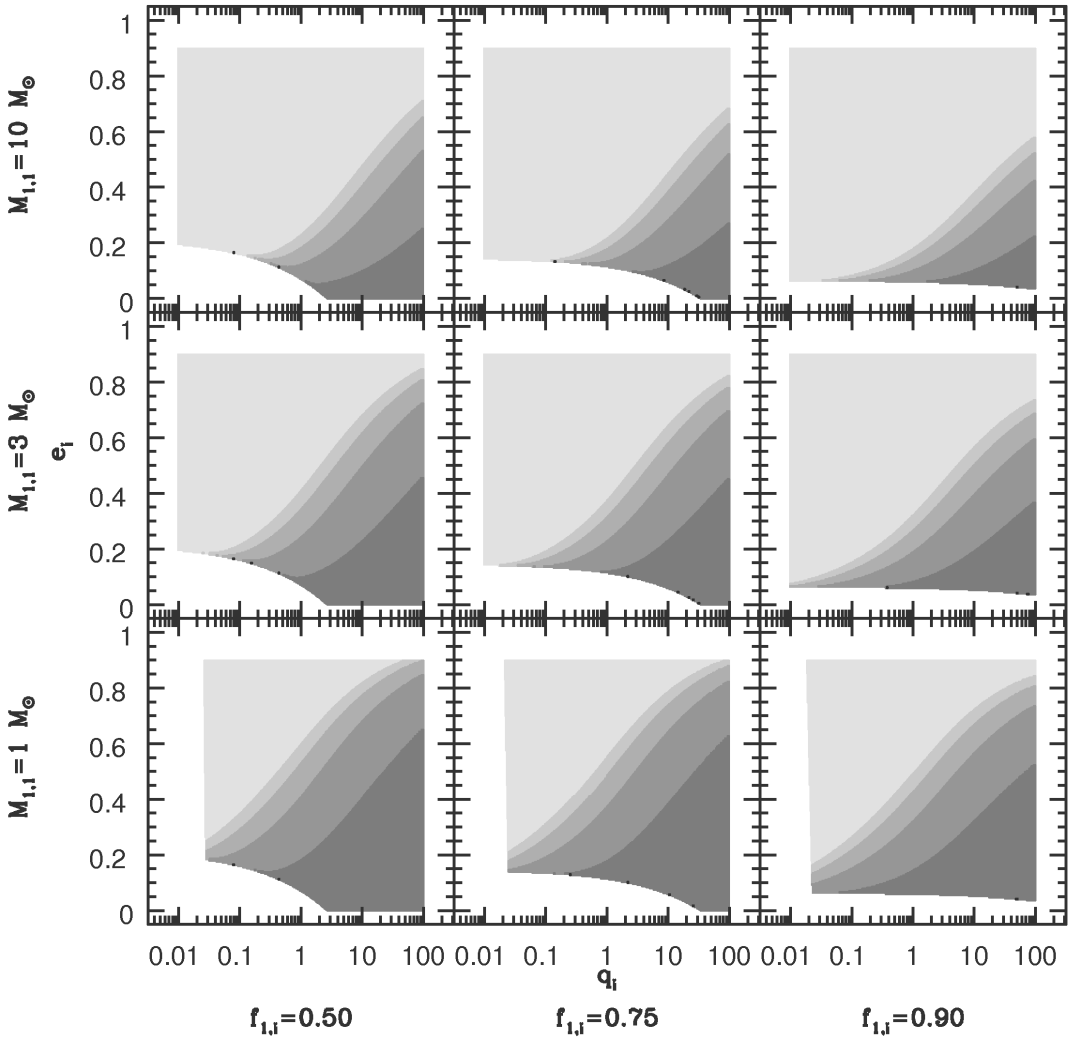

FIG. 8.— Same as Figure 7, but for the evolution of the orbital eccentricity e.

TABLE 1
INITIAL AND FINAL BINARY PARAMETERS FOR THE EVOLUTIONARY SEQUENCES SHOWN IN FIGURES 9 AND 10

	$M_1\,(M_\odot)$		$M_2\,(M_\odot)$		q		$a\,(R_\odot)$		e		f_1		f_2		$t_{\rm final}$
System	Initial	Final	Initial	Final	Initial	Final	Initial	Final	Initial	Final	Initial	Final	Initial	Final	(Gyr)
A	1.00	0.78	20.00	20.02	0.05	0.04	9.31	11.65	0.025	0.000	0.50	0.20	1.00	1.50	0.14
B	1.00	0.81	10.00	10.19	0.10	0.08	7.85	9.63	0.050	0.000	0.50	0.23	1.00	1.58	0.13
C	1.00	0.99	0.25	0.26	4.00	3.81	3.24	3.12	0.050	0.000	0.75	0.75	1.00	2.00	0.01
D	3.00	2.38	15.00	15.62	0.20	0.15	2.26	28.56	0.050	0.000	0.75	0.31	1.00	2.49	0.41
E	10.00	9.97	1.00	1.03	10.00	9.68	19.78	19.32	0.025	0.000	0.90	0.91	1.00	2.57	0.02
F	1.00	1.00	0.25	0.25	4.00	4.00	3.16	3.07	0.050	0.000	0.50	0.53	1.00	1.06	0.01
G	3.00	3.00	5.00	5.00	0.60	0.60	2.71	2.41	0.400	0.234	0.75	0.78	1.00	1.39	1.42
H	3.00	3.00	0.50	0.50	6.00	6.00	17.41	14.23	0.400	0.063	0.90	0.88	1.00	1.66	0.32
I	10.00	10.00	100.0	100.0	0.10	0.10	266.55	253.65	0.800	0.789	0.50	0.58	1.00	1.02	11.9

NOTE. — M_1 is the mass of the donor star, M_2 the mass of the companion, $q = M_1/M_2$ the mass ratio, a the semi-major axis, e the orbital eccentricity, f_1 the rotational angular velocity of the donor star in units of the orbital angular velocity at periastron, f_2 the rotational angular velocity of the donor star in units of the orbital angular velocity at periastron, and $t_{\rm final}$ the time at which the calculation was terminated.

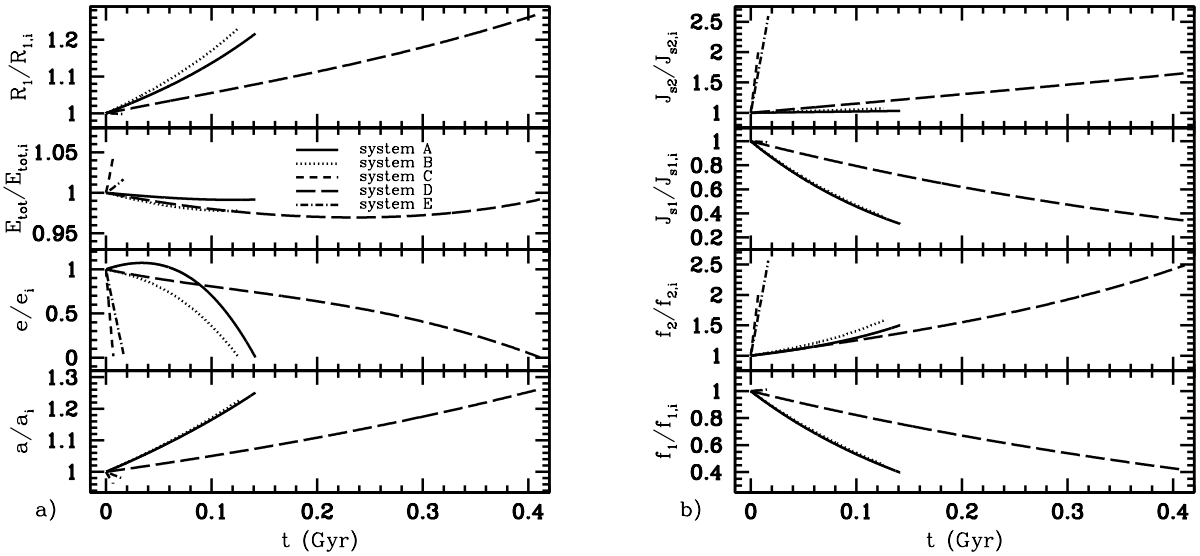

FIG. 9.— Evolution of orbital parameters as a function of time for systems undergoing direct impact accretion. The y-axes show the fractional change in the parameters relative to their initial value. The initial and final values for some of the system parameters are shown in table 1. In **(a)**, we show, from top to bottom, the radius of star 1, the total energy of the system (orbital plus the spin of each component), the eccentricity, and the semi-major axis. In **(b)**, we show, from top to bottom, the spin angular momentum of star 2, the spin angular momentum of star 1, and the rotation rates of stars 2 and 1.

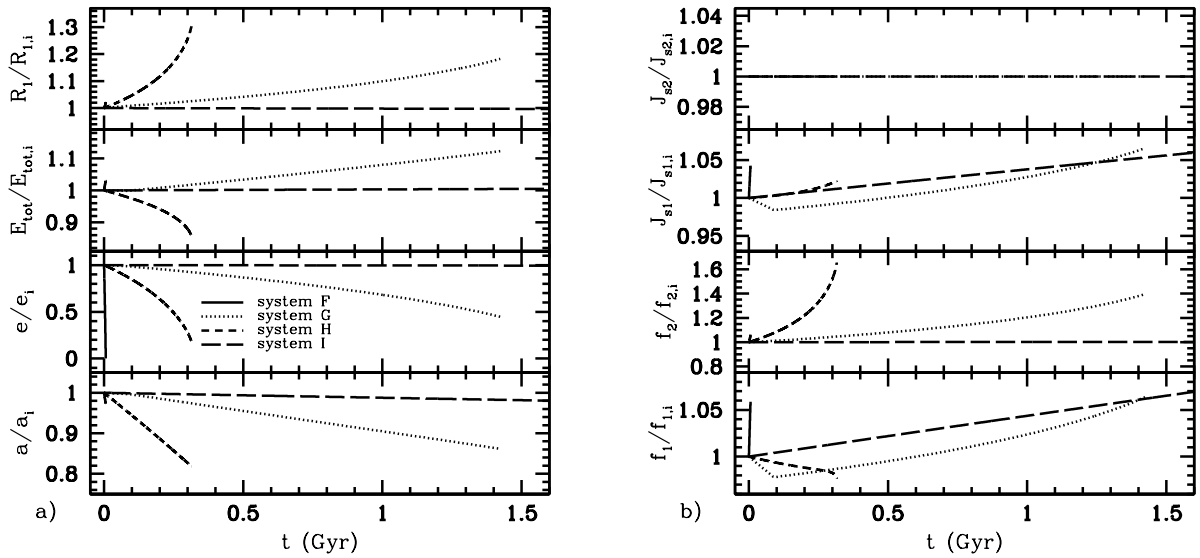

FIG. 10.— Same as Figure 9, but for systems undergoing self-accretion.

f_1 and f_2, are shown as a function of time for systems undergoing direct impact accretion and self-accretion, respectively. The evolutionary sequences were calculated for up to four mass transfer timescales $M_1/|\dot{M}_0|$ (systems G and I) or until the binary circularized (systems A through F), whichever occurred first. For system H, the calculation was terminated at time $t = 0.32\,\mathrm{Gyr}$ when it ceased to be a self-accretion system. The initial and final parameters of the nine evolutionary sequences shown are summarized in Table 1.

The direct impact systems shown in Figure 9 all circularize within a few Gyr or less after the start of mass overflow. In the case of system A, the eccentricity initially grows, reaching a peak $e_{\max} = 0.0268$ at $t = 0.034\,\mathrm{Gyr}$, before circularizing at an increasingly rapid rate. The semi-major axes generally increase, except for systems C and E, as expected for binaries with mass ratios $q > 1$ and almost circular orbits. Mass loss from the donor star and the growth of the donor's radius, which is required to track the growing effective Roche lobe, furthermore decrease the donor's rotation rate to significantly sub-synchronous values at the end of the evolutionary sequence for systems A, B, and D. For systems C and E, mass transfer to the less massive star 2 causes the semi-major axis to decrease, increasing the orbital angular velocity at periastron, and thereby effectively *increasing* the donor rotation rate. This in turn causes the effective Roche lobe radius of the donor to shrink. We note that in all five cases shown, the end of the evolutionary sequence corresponds to the time at which the binary becomes circular, not to the cessation of mass transfer in the binary system.

The self-accretion systems shown in Figure 10 decrease their eccentricity as a result of mass overflow, though system I has an evolutionary timescale for the orbital eccentricity much longer than a Hubble time (see Figure 8). The orbital semi-major axes always decrease, while the donor rotation rates can increase as well as decrease during the course of mass overflow. There is no change in the spin angular momentum of star 2 since there is no mass transferred. In this case, the change in f_2 is due entirely to the change in the orbital angular velocity at periastron. In the case of system G, the donor initially spins down by a few per cent relative to the rotational angular velocity at periastron, but reverses its spin evolution after about 100 Myr. At the end of the evolutionary phase shown (corresponding to four mass transfer time scales), the donor is spinning super-synchronously at the periastron of the binary orbit. The donor rotation rate for System H slowly decreases until just past $t \approx 0.3\,\mathrm{Gyr}$, at which time it rapidly plunges to very low rotation rates. We note that the physical rotation rate of this donor star never actually decreases, and that the decrease in f_1 is caused by the orbital angular velocity at periastron increasing at a rate faster than the actual rotation rate of the donor star. The rapid decrease starts a few orbits before the system transitions from a self-accretion system to a system in which the ejected matter impacts neither star 1 nor star 2 during the course of one binary orbit. Since our code is currently not equipped to deal with the evolution of systems like this, we terminated the calculation at this point.

We note that at every step of the orbital evolution calculations, both the total linear and angular momenta of the system remain constant. However, mass overflow can exchange momentum between the spins of the binary components and the orbit. We particularly find that, contrary to past assumptions (for example, see Verbunt & Rappaport 1988; Marsh et al. 2004), direct impact accretion does not necessarily provide a sink of orbital angular momentum (see also Motl et al. 2007). Instead, the transferred matter contains both spin and orbital angular momentum from the donor star, part of which can be returned to the orbit upon accretion. This makes it possible for the orbital angular momentum to increase at the expense of the spin angular momentum of the donor. The impact of this result on the stability of mass overflow in close binaries such as double white dwarfs will be the subject of a forthcoming investigation.

Lastly, we can see from Figures 9 and 10 that the total energy of the system can change significantly over the course of its lifetime. Due to our assumption that the particle is ejected and accreted perfectly inelastically (i.e., with no loss of momentum), it is impossible to conserve the total system energy as well. Even in the case of self-accretion where the mass of star 1 is unchanged the ejected particle self-accretes with a different position and velocity than that with which is was ejected. For the systems tested here, the total energy can change by as much as 10% or more, and can either increase or decrease depending on the system parameters. The energy added or subtracted from the system might be accompanied by a commensurate change in the thermal energy of the stars' envelopes.

5. DISCUSSION AND CONCLUSIONS

In this paper, we extended our previous work on mass transfer in eccentric binaries by using ballistic trajectory calculations to determine the parameter space for different outcomes of mass overflow. Assuming mass overflow takes place through Roche lobe overflow at the periastron of the binary orbit, we explored a broad parameter space to determine the conditions under which mass overflow leads to direct impact accretion onto the donor's companion or to fallback onto the donor star ("self-accretion"). The results presented in this paper along with those presented in Sepinsky et al. (2007a,b, 2009), provide a self-consistent picture of the orbital evolution of eccentric effective Roche lobe overflowing binary star systems as a function of their initial orbital parameters. Until now, such a picture has been lacking both in binary stellar evolution and binary population synthesis codes.

We find that systems with a large initial eccentricity ($e_i \gtrsim 0.2$) or a donor initially rotating near synchronicity ($f_{1,i} \gtrsim 0.8$) are always expected to undergo self-accretion. Direct impact accretion or disk formation is expected to occur mainly for systems with low eccentricities, low mass ratios, and substantially subsynchronously rotating donor stars. Furthermore, self-accretion is found to always decrease the orbital eccentricity, and can do so over timescales ranging from less than a Myr to more than a Gyr depending on the initial binary parameters and the chosen mass overflow rate.

To illustrate the applicability of the presented formalism, we calculated the orbital evolution due to mass overflow for eccentric binaries consisting of an evolved main sequence donor and a zero-age main sequence accretor as

a function of the initial binary parameters. For binaries undergoing direct impact accretion, mass transfer can increase as well decrease the initial orbital semi-major axis and eccentricity, while for binaries undergoing self-accretion, mass overflow always decreases both the initial orbital semi-major axis and eccentricity. For a mass overflow rate of $\dot{M}_0 = -10^{-9}\,M_\odot\,\mathrm{yr}^{-1}$, the time scales of orbital evolution can range from less than 1 Gyr to more than a Hubble time.

In this exploratory study, both the donor star and the accretor were treated as rigid spheres. The results presented therefore do not account for orbital evolution due to tidal torques or for the radial response of the donor star to mass loss. Our calculations nevertheless clearly illustrate that mass overflow leading to direct impact accretion or self-accretion can both enhance or counteract the effects of tides in eccentric effective Roche lobe overflowing binaries. A similar conclusion was reached by Sepinsky et al. (2007b, 2009) for binaries in which mass transfer leads to the formation of an accretion disk. As one of the next steps in our investigation, we will implement more realistic stellar models in our ballistic particle trajectory code and examine the effects of tides and stellar evolution on mass transfer in eccentric binaries.

While not discussed in detail here, we also find that direct impact accretion does not necessarily deposit all of the accreted matter's angular momentum into the spin of the accretor. Instead, some of this angular momentum, which originated from both spin and orbital angular momentum of the donor star, is deposited into the accretor's spin while the remaining part is returned to the orbit. This is in stark contrast to commonly adopted assumptions in stability studies of mass transfer in ultra-compact binaries (e.g., Verbunt & Rappaport 1988; Marsh et al. 2004). The possibility of avoiding strong orbital angular momentum loss during direct impact accretion is particularly relevant in predicting expected gravitational wave detection rates from mass-transferring double white dwarfs (AM CVn stars) by the Laser Interferometer Space Antenna (LISA).

We thank Christopher Deloye for numerous useful discussions, Francesca Valsecchi for the use of her C implementation of Steffen's (1990) interpolation algorithm used to calculate the time derivatives of the orbital elements, and Christopher Tout for a number of useful suggestions. This work is partially supported by a NASA Graduate Fellowship (NNG04GP04H/S1) to J.S., and a NSF CAREER Award (AST-0449558), a Packard Fellowship in Science and Engineering, and a NASA ATP Award (NAG5-13236) to V.K.

REFERENCES

Avni, Y. 1976, ApJ, 209, 574
Church, R. P., Dischler, J., Davies, M. B., Tout, C. A., Adams, T., & Beer, M. E. 2009, MNRAS, 394
Galassi, M., J., D., Theiler, J., Gough, B., Jungman, G., Booth, M., & Rossi, F. 2006, GNU Scientific Library Reference Manual (2nd Ed.) (Network Theory Ltd.)
Hadjidemetriou, J. D. 1969, Ap&SS, 3, 330
Hurley, J. R., Pols, O. R., & Tout, C. A. 2000, MNRAS, 315, 543
Layton, J. T., Blondin, J. M., Owen, M. P., & Stevens, I. R. 1998, New Astronomy, 3, 111
Limber, D. N. 1963, ApJ, 138, 1112
Lubow, S. H., & Shu, F. H. 1975, ApJ, 198, 383
Marsh, T. R., Nelemans, G., & Steeghs, D. 2004, MNRAS, 350, 113
Motl, P. M., Frank, J., Tohline, J. E., & D'Souza, M. C. R. 2007, ApJ, 670, 1314
Nelemans, G., Portegies Zwart, S. F., Verbunt, F., & Yungelson, L. R. 2001, A&A, 368, 939
Plavec, M. 1958, Mémoires de la Société Royale des Sciences Liège, 20, 411
Regös, E., Bailey, V. C., & Mardling, R. 2005, MNRAS, 358, 544
Sepinsky, J. F., Willems, B., & Kalogera, V. 2007a, ApJ, 660, 1624
Sepinsky, J. F., Willems, B., Kalogera, V., & Rasio, F. A. 2007b, ApJ, 667, 1170
—. 2009, ApJ, 702, 1387
Steffen, M. 1990, A&A, 239, 443
Sterne, T. E. 1960, An introduction to celestial mechanics (Interscience Tracts on Physics and Astronomy, New York: Interscience Publication, 1960)
Verbunt, F., & Rappaport, S. 1988, ApJ, 332, 193